IEEE Access
Multidisciplinary | Rapid Review | Open Access Journal

Received April 14, 2020, accepted April 21, 2020, date of publication May 6, 2020, date of current version May 18, 2020.

Digital Object Identifier 10.1109/ACCESS.2020.2991842

No-Reference Quality Assessment for Contrast-Distorted Images

YUTAO LIU AND XIU LI, (Member, IEEE)
Department of Information Science and Technology, Tsinghua Shenzhen International Graduate School, Shenzhen 518055, China
Corresponding authors: Yutao Liu (liuyutao2008@gmail.com) and Xiu Li (li.xiu@sz.tsinghua.edu.cn)

This work was supported in part by the China Postdoctoral Science Foundation under Grant 2019M650686 and in part by the National Science Foundation of China under Grant 41876098.

ABSTRACT Contrast distortion is a common distortion type in the image applications. However, there are still very limited approaches proposed for quantifying the quality of the contrast-distorted images reliably. In this paper, we devise a novel no-reference/blind quality assessment method for those contrast-distorted images. In the proposed method, we characterize the image quality by deeply investigating multiple contrast distortion-relevant properties of the image, i.e., spatial characteristics, image histogram, visual perception characteristics and chrominance, which can describe the image quality more comprehensively and precisely. Accordingly, a series of quality-aware features are developed to characterize the contrast-distorted image quality properly. Support vector regression (SVR) is then employed to integrate all the extracted features and infer the image quality score. Extensive experiments conducted on the standard contrast-distorted image databases/datasets demonstrate that the proposed method achieves superior prediction performance to the state-of-the-art NR quality assessment models on evaluating the contrast-distorted image quality.

INDEX TERMS Image quality assessment, no-reference/blind, contrast distortion, free-energy theory, natural scene statistics (NSS).

I. INTRODUCTION

Image quality assessment (IQA) is a fundamental issue in the image processing field. Since the image is usually consumed by humans, subjective quality assessment by humans always represents the most reliably way [1]. But subjective assessment manner suffers from obvious drawbacks. It's always cumbersome, time-consuming and can't be applied in those applications with high real-time requirement. By contrast, objective IQA that resorts to mathematical models is more appropriate for quality evaluation and has aroused wide attention in these years. Generally, according to the requirement for the original image, existing objective IQA methods can be classified into three categories, i.e., full-reference (FR) IQA, reduced-reference (RR) IQA and no-reference (NR)/blind IQA. FR IQA methods compute the image quality under the condition that the original image is fully accessible [2], [3]. RR IQA methods use partial information of the original image for quality evaluation [4]–[6]. NR IQA methods aim to estimate the image quality without referring to the original image [7]–[9].

The most widely-adopted FR IQA metrics are the peak signal-to-noise ratio (PSNR) and the structural similarity index (SSIM) [2]. Specifically, PSNR measures the image quality by directly computing the difference between the original image and the distorted image, which is simple and explicit for use. SSIM deduces the image quality through computing the structural similarity between the original image and the distorted image, based on the assumption that the human visual system (HVS) is highly sensitive to the structures in the image. Based on other design philosophies, a lot of successful FR IQA methods have also been constructed and facilitated the FR IQA research significantly [10]–[12].

Compared with FR IQA, RR IQA evaluates the image quality by referring to partial information of the original image. In [13], Wang *et al.* reported an effective RR IQA approach by formulating the marginal distribution of the wavelet coefficients to design the quality-aware features. Reduced reference entropic differencing (RRED) was developed by calculating the differences between wavelet coefficients

The associate editor coordinating the review of this manuscript and approving it for publication was Menghan Hu.

entropies of the reference and distorted images [4]. In [14], Liu *et al.* established a RR IQA method in free-energy principle and sparse representation. In [15], Min *et al.* proposed a RR quality index based on extracting the saliency features of the image. In [16], a RR quality metric that combines the multi-channel decomposition theory and the free-energy principle was proposed, in which the image was firstly decomposed into subbands with the discrete Haar wavelet transform to extract the free-energy-based features, then SVR was used to regress the features to the image quality score.

NR IQA is proposed to estimate the image quality when the original image is unavailable. As there's no reference information to use, the design of NR IQA methods is much more challenging than the FR and RR IQA methods [17]–[20]. Traditional popular solution to NR IQA follows two successive steps. In the first step, quality-aware features are extracted to characterize the image quality degradations. In the second step, SVR is employed to regress the extracted features to the image quality score. Representative works are reviewed as follows. In [21], Saad *et al.* dug into the DCT coefficients of the image to extract the NSS features for quality estimation. In [22], Moorthy *et al.* formulated the statistical regularities of the wavelet coefficients to estimate the image quality degree. In [23], Mittal *et al.* designed the quality-aware features in the spatial domain of the image. In [24], Li *et al.* used both local phase and local amplitude for evaluating the quality of the multiply distorted images. In [25], Min *et al.* introduced the multiple pseudo reference images by degrading the distorted image in different ways, based on which designed the quality-aware features for NR IQA. Apart from using SVR as the regressor for quality evaluation, in [7], [26], a multivariate Gaussian (MVG) model was learned from a set of pristine images, which servers as the ''reference'' information for defining the image quality. In [27], Xue *et al.* established a quality-aware clustering (QAC) method, in which a set of centroids of different quality levels was learned to compute the image quality. Recently, with the rapid development of deep learning theory and technologies, IQA researchers have introduced deep learning into NR IQA, which greatly promotes the development of NR IQA. In [28], Ma *et al.* created a vast amount of quality-discriminable image pairs (DIPs) which serve as the training data and learned a DIP inferred quality (dipIQ) index through RankNet. In [29], Yan *et al.* proposed a two-stream convolutional neural network (CNN) framework to learn more effective feature representations for NR IQA. In [30], Kim *et al.* proposed a deep CNN-based blind IQA approach, in which they firstly learned to predict the objective error map, then learned to predict the image quality score.

The image contrast is an important attribute of the image, which has a significant effect on the visual perception behaviors of the human brain, such as image quality perception [31], [32], visual saliency [33], etc. For example, in [34], Zhu *et al.* indicated that more visual attentions focus on those areas of high contrast between the center and peripheral visual fields, based on which contrast-related features were thus developed to predict the salient regions. The color contrast was measured to enhance the visual saliency prediction in 360 degree images [33]. However, during the image acquisition process, the distortion of the image contrast is often introduced due to the limitation of the photographing device or bad photographing conditions, which affects the image quality severely. Despite the prosperity of the IQA research, the issue of quality assessment for the contrast-distorted images is still overlooked [35]. Only several specialized IQA methods in the IQA researches have been reported to evaluate the quality of the contrast-distorted images. In [36], Wang *et al.* proposed a local patch-based quality index to quantify the quality of the contrast-distorted images, where the image patch was firstly decomposed into its mean intensity, signal strength and signal structure components, then the image quality score was computed by measuring the distortions of the three components. In [32], Fang *et al.* extracted NSS features to characterize the contrast distortion and presented a dedicated NR quality metric for the contrast-distorted images. In [35], Gu *et al.* constructed a RR contrast-distorted image quality metric by analyzing the phase congruence and statistics information of the image histogram. In [31], Gu *et al.* further learned a NR quality assessment model for the contrast-distorted images with big data.

Although the above quality assessment schemes for the contrast-distorted images have been proved to be effective, their prediction performance is still limited. The primary reasons can be summarized as follows. First, most of the existing contrast-distorted IQA methods only investigate a small number of image properties for quality estimation, which can't evaluate the image quality adequately. Second, the quality perception mechanism of the human brain is rarely explored, which limits the prediction accuracy of the developed objective algorithms inevitably. Third, chrominance of the image is closely related to the image quality. However, the characterization of the chrominance is often ignored. To tackle the existing problems and develop more effective quality metric for the contrast-distorted image, in this paper, we develop a novel NR contrast-distorted image quality assessment scheme. Overall, rather than investigating single image property for quality evaluation, we investigate multiple aspects of the image that are quite indicative to the contrast distortion, i.e., spatial characteristics, image histogram, visual perception and chrominance, which is able to measure the image quality comprehensively and more precisely. In particular, we deeply investigate the human brain perception mechanism based on the free-energy principle and also thoroughly characterize the chrominance of the image for quality evaluation. A set of quality-aware features are thus designed to quantify the image quality degradations appropriately. Then SVR is employed to regress all the features to the image quality score. We name our proposed method as Blind Contrast-distorted Image Quality Model, or abbreviated as BCIQM. Extensive tests executed on three standard contrast-distorted image databases/datasets,

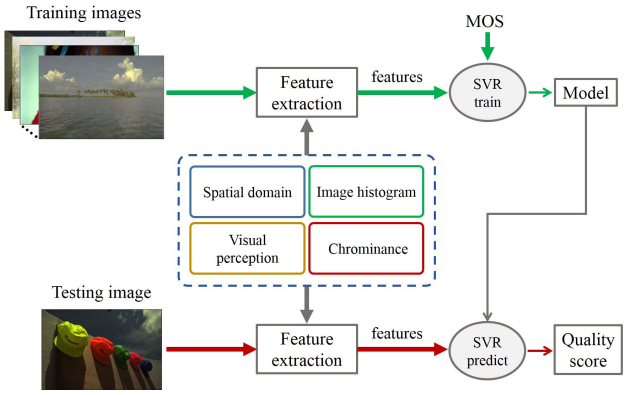

FIGURE 1. The overall framework of the proposed method.

i.e., CCID2014, TID2013 and CSIQ demonstrate that the proposed BCIQM outperforms state-of-the-art general-purpose and contrast-distortion NR IQA methods on predicting the quality of the contrast-distorted images.

The remainder of this paper is organized as follows: In Section II, we introduce the proposed BCIQM for contrast-distorted images in detail. In Section III, we present the experimental results and necessary analysis to verify the effectiveness and superiority of BCIQM. In Section IV, we conclude this paper.

II. PROPOSED METHOD

For characterizing the quality of the contrast-distorted image precisely, measuring single aspect of the image is far from enough [31]. Therefore, in this paper, we investigate multiple aspects of the image that are affected by the contrast distortion and devise a group of quality-aware features to characterize the contrast distortion effectively. After feature extraction, we employ SVR to regress those features onto the image quality level. For better understanding of the proposed scheme for contrast-distorted images, we show its overall framework in Fig. 1 clearly. To be specific, we train a quality prediction model with SVR on a set of training images and then employ it to predict the quality of a given testing image.

A. FEATURE EXTRACTION IN THE SPATIAL DOMAIN

Features extracted in the image spatial domain have been proved to be highly effective to characterize the image quality [7], [23], [26]. In addition, spatial features are often efficient for computation. Therefore, we at first exploit spatial features of the image for quality estimation. Specifically, we extract two types of spatial features that convey close relationships with the contrast deviation.

The first type of feature we extract is the gradient magnitude (GM). The GM feature can describe the structures of the image exactly, which contains rich information for quality perception [2]. More importantly, contrast distortion can be well captured by the GM feature [10]. To extract the GM feature, we firstly extract the image gradients by convolving the distorted image I with the Prewitt operator along the vertical and horizontal directions as:

$$G_x(I) = \frac{1}{3}\begin{bmatrix} 1 & 0 & -1 \\ 1 & 0 & -1 \\ 1 & 0 & -1 \end{bmatrix} \otimes I \tag{1}$$

$$G_y(I) = \frac{1}{3}\begin{bmatrix} 1 & 1 & 1 \\ 0 & 0 & 0 \\ -1 & -1 & -1 \end{bmatrix} \otimes I \tag{2}$$

where $G_x(I)$ and $G_y(I)$ are the vertical and horizontal gradients, "$\otimes$" denotes the convolution operator. Then GM image of I can be calculated as:

$$GM = \sqrt{G_x^2 + G_y^2} \tag{3}$$

where GM refers to the GM image. Here, we further calculate the mean value of the obtained GM image and use it to characterize the image contrast distortion.

In Fig. 2, we illustrate the potential effectiveness of the GM features in characterizing the contrast distortion with an example. In the first row, we show four images which are the original image without contrast distortion, slightly contrast-distorted image, moderately contrast-distorted image and severely contrast-distorted image, respectively. The second row are their corresponding GM images, m refers to the mean value of the GM image. This figure reveals some meaningful observations. First, compared with the original image, the contrast-distorted images are all of low visual quality, which indicates that contrast plays an important role in affecting the image quality. Second, by observing the GM images, we can find that GM can extract the structures of the image exactly. Third, as the contrast distortion degree increases, the GM image is more deviated from the original one, for example, in the regions marked by the yellow rectangles. In addition, the mean values of the distorted GM images vary monotonously according to the variation of the contrast distortion level. These observations manifest the effectiveness of the GM image and its mean value in characterizing the contrast distortion intuitively.

Apart from computing the GM feature to indicate the contrast variation, we further inspect the pixel differences between the image adjacent pixels of the contrast-distorted image, which is also modified by the contrast distortion. Specifically, we firstly calculate the differences between the current pixel and its adjacent left, right, top and bottom pixels in the contrast-distorted image. Then we calculate the weighted sum of the pixel differences to measure the overall contrast distortion degree as:

$$S_w = \sum_{\delta} \delta(m,n)^2 P_\delta(m,n) \tag{4}$$

where $\delta(m,n) = |m-n|$ refers to the difference between two adjacent pixels, $P_\delta(m,n)$ is the distribution probability of the difference that equals $\delta(m,n)$. In Fig. 3, we show $P_\delta(m,n)$ against $\delta(m,n)$ of the original, slightly contrast-distorted, moderately contrast-distorted, severely contrast-distorted images shown in the first row of Fig. 2. As observed, the adjacent pixel difference distribution varies

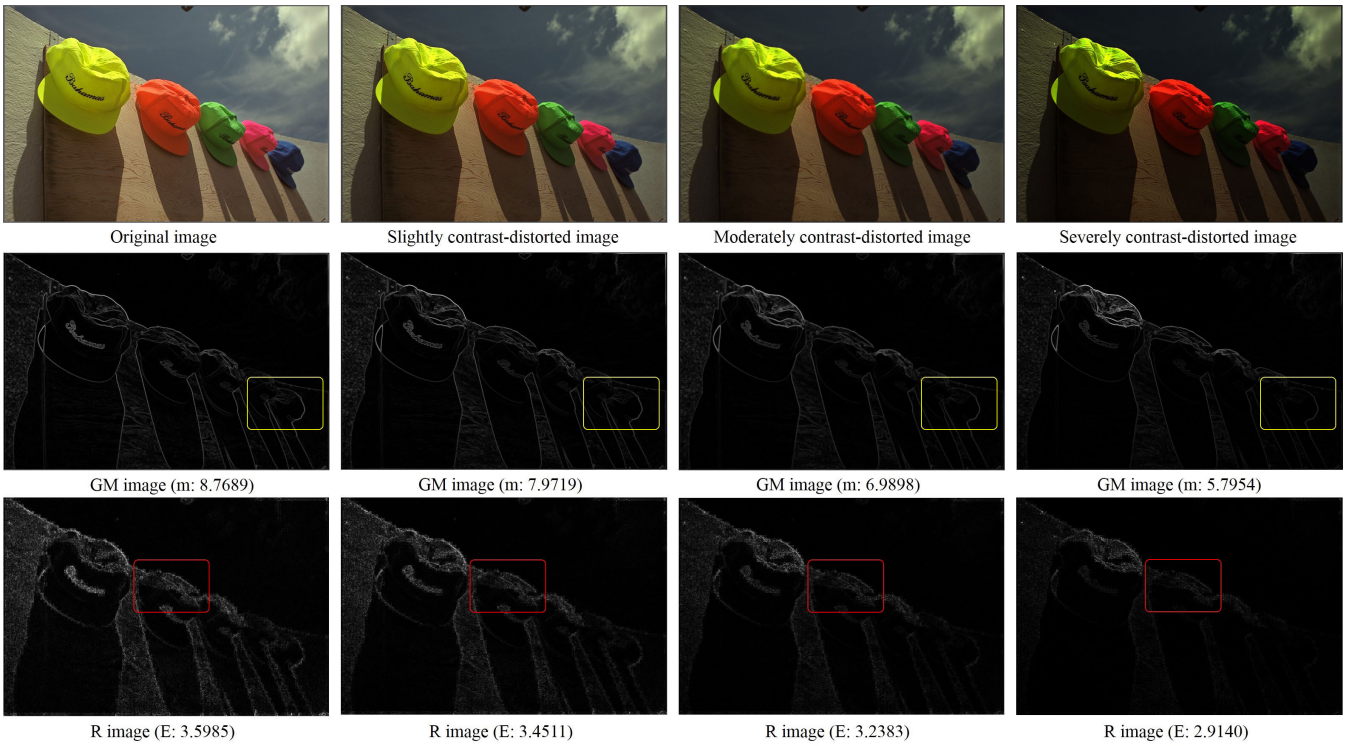

FIGURE 2. The GM maps and the prediction residual (R) images of the original image and the contrast-distorted images.

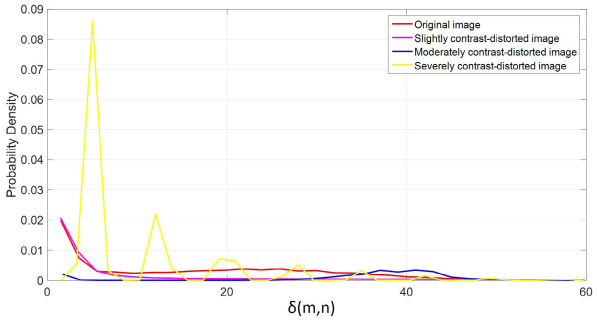

FIGURE 3. The adjacent pixel difference distributions of the original, slightly contrast-distorted, moderately contrast-distorted, severely contrast-distorted images.

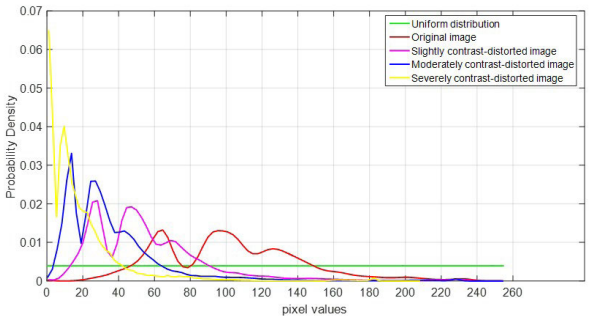

FIGURE 4. The probability densities of the uniform distribution and the original, slightly contrast-distorted, moderately contrast-distorted, severely contrast-distorted images.

in line with the variation of the contrast distortion level, which intuitively demonstrates the availability of the adjacent pixel difference in characterizing the contrast distortion in the image.

B. FEATURE EXTRACTION FROM THE IMAGE HISTOGRAM

The image histogram is used to represent the brightness distribution of the image, which is widely used in image processing. As we know, the histogram of a low-contrast image tends to be askew or deviated from the uniform distribution. Here, we use an example to illustrate this fact. In Fig. 4, we plot the probability densities of the uniform distribution and the original, slightly contrast-distorted, moderately contrast-distorted, severely contrast-distorted images which are the images shown in the first row of Fig. 2, respectively. As we can observe, the curve of the probability density tends to become more and more askew or deviated from the uniform distribution as the contrast distortion degree increases. Therefore, the deviation degree of the image histogram against the uniform distribution provides a good quantitative measure of the contrast-distorted image quality [37]. Suppose $\mathbf{h}$ and $\mathbf{u}$ to be the contrast-distorted image histogram and the uniform distribution respectively, then we measure the distance between $\mathbf{h}$ and $\mathbf{u}$ with the well-known K-L divergence, which is often employed to evaluate the distance between two distributions, defined as:

$$D_{KL}(\mathbf{h}\|\mathbf{u}) = -\int h(t)\log u(t)dt + \int h(t)\log h(t)dt \quad (5)$$

as the pixel value of the image is in [0,255], the probability density $u(t)$ of $\mathbf{u}$ equals $1/255$. Then the first term of the above equation equals $-\log 1/255$ actually, which is a constant and can be omitted. Therefore, the K-L divergence between $\mathbf{h}$ and $\mathbf{u}$ can be further derived as $\int h(t)\log h(t)dt$. However, the K-L divergence is non-symmetric and may cause some instability. Therefore, we adopt another symmetrized and smoothed version that is derived from the K-L divergence, namely the Jensen-Shannon (J-S) divergence to compute the distance between $\mathbf{h}$ and $\mathbf{u}$:

$$D_{JS}(\mathbf{h},\mathbf{u}) = \frac{D_{KL}(\mathbf{h}\|\mathbf{m}) + D_{KL}(\mathbf{u}\|\mathbf{m})}{2} \tag{6}$$

where $\mathbf{m} = \frac{1}{2}(\mathbf{h}+\mathbf{u})$. Then we employ $D_{JS}(\mathbf{h},\mathbf{u})$ to estimate the quality of the contrast-distorted image from the perspective of image histogram.

C. CHARACTERIZATION OF THE VISUAL PERCEPTION

The image quality is actually an outcome of the interaction between the human brain and the external image signal, or visual perception [5]. However, few NR IQA of contrast-distorted images investigated the visual perception process to characterize the image quality. In this work, we explore the visual perception of the human brain deeply and thus characterize the image quality from the perspective of visual perception.

Specifically, in brain theory and neuroscience, a newly-proposed free-energy principle that unifies several brain theories and physical findings was proposed to explain the human action, perception and learning [38], [39]. The free-energy principle indicates that the perception or understanding of the visual scene is an active inference activity which is controlled by an internal generative model (IGM) [5], [40]. More specifically, through the IGM, the human brain yields the corresponding representations of the input visual signals for perception. The perceptual quality of the image is thus closely related to the discrepancy between the image and its brain representation [5], [14]. For characterizing the visual perception process, we need to figure out the IGM in the first place. However, the determinate form of the brain IGM hasn't been revealed till now as the human brain is too complicated and far beyond our current knowledge. To tackle this problem, researchers have resorted to existing model to approximate the IGM for modeling visual perception [5], [41]. In earlier works, the auto-regressive (AR) model was always adopted as the IGM as it's flexible to represent natural images. However, in [42], [43], Olshausen *et al.* found that the receptive fields of simple cells in mammalian primary visual cortex of the brain can be characterized as being spatially localized, oriented and bandpass. Then they further indicated that sparse representation for natural images could agree with those properties exactly observed in the visual cortex [44]–[46]. Inspired by these neurobiological findings, in our earlier work [3], [14], we approximated the IGM with sparse representation and verified that it is indeed much more effective and efficient than the AR model for image quality evaluation. Therefore, in this work, we still employ sparse representation to approximate the IGM of the human brain.

To represent an input image I sparsely, we at first extract a patch $\mathbf{x}_k \in \mathbb{R}^{B_s}$ from I with an extraction operator $\mathbf{R}_k(\cdot)$, then the sparse representation of $\mathbf{x}_k$ over an over-complete dictionary $\mathbf{D} \in \mathbb{R}^{B_s \times M}$ is actually to calculate a vector $\boldsymbol{\alpha}_k \in \mathbb{R}^M$ to represent $\mathbf{x}_k$, satisfying that the elements in $\boldsymbol{\alpha}_k$ are mostly zero or close to zero, which can be formulated as:

$$\boldsymbol{\alpha}_k^* = \underset{\boldsymbol{\alpha}_k}{\operatorname{argmin}} \frac{1}{2}\|\mathbf{x}_k - \mathbf{D}\boldsymbol{\alpha}_k\|_2 + \lambda\|\boldsymbol{\alpha}_k\|_0 \tag{7}$$

where the first term denotes the representation fidelity, the second term restricts the sparsity of the vector $\boldsymbol{\alpha}_k$. λ is a constant to adjust the significance of the two terms. $\|\cdot\|_0$ refers to the l^0 norm which directly counts the non-zero elements in $\boldsymbol{\alpha}_k$. By solving the above equation, we can obtain the sparse vector $\boldsymbol{\alpha}_k^*$ for representing $\mathbf{x}_k$. Then the sparse representation of the entire image I can be calculated as:

$$I' = \sum_{k=1}^{n} \mathbf{R}_k^T(\mathbf{D}\boldsymbol{\alpha}_k^*)./\sum_{k=1}^{n} \mathbf{R}_k^T(\mathbf{1}_{B_s}) \tag{8}$$

where I' refers to the sparse representation of image I, which serves as the brain representation of I. "./" refers to the element-wise division of two matrices, n is the total number of the image patches. $\mathbf{R}_k^T(\cdot)$ is the transpose operation of $\mathbf{R}_k(\cdot)$, which puts $\mathbf{x}_k$ to its original position in the image. $\mathbf{1}_{B_s}$ refers to the vector of size B_s whose elements are all 1. The second term $\sum_{k=1}^{n} \mathbf{R}_k^T(\mathbf{1}_{B_s})$ in the above equation counts the number of the patches that are put back onto the same position in the represented image I'. Dividing the first term by the second term means taking the mean value of the patches as the final value on the same position.

According to the free-energy principle, the representation discrepancy between the input image and its brain representation is believed to be closely related to the quality of human perceptions. More precisely, the quality of perceptions can be quantified mathematically by the uncertainty of the prediction discrepancy [5], [14]. Accordingly, we firstly define the prediction residual as the discrepancy between the image and its brain representation:

$$R = |I - I'| \tag{9}$$

where R refers to the prediction residual. "$|\cdot|$" is the magnitude operation. Then the uncertainty of R can be measured by its entropy, defined as:

$$E = -\sum_{i=0}^{255} p_i \log_2 p_i \tag{10}$$

where E represents the entropy of R, p_i is the probability density of ith gray scale in R. In the third row of Fig. 2, we give the calculated prediction residual images R and the corresponding E values of the original and contrast-distorted images. Note that we have expanded the pixel values in R by three times for convenient observation. As illustrated, the residual image R degenerates gradually with the increase

of the contrast distortion level, for example, in the regions marked by the red rectangles. The value of E also changes monotonously as the contrast distortion degree increases. Therefore, we employ E as our visual perception feature for characterizing the perceptual quality of the contrast-distorted image.

D. CHARACTERIZATION OF CHROMINANCE

It's widely accepted that chrominance of the image plays a significant role in evaluating the image quality [31], [47]. Similarly, for contrast-distorted images, the chrominance of the image is often poor, which leads to the image quality degradations. To extract the chrominance information, we at first transform the image from the RGB color space to the perceptually relevant CIELAB color space, which includes one luminance channel 'L' and two chrominance channels 'A' and 'B' [48]. More specifically, 'L' channel represents the brightness of the image. 'A' channel is relative to the red/magenta and green and 'B' channel is relative to yellow and blue. As in [49], we compute the perceived intensity of the chrominance by:

$$C = \sqrt{A^2 + B^2} \tag{11}$$

where C denotes the chrominance intensity of the image. Previous studies have demonstrated that the locally mean subtracted and contrast normalized (MSCN) coefficients of the chrominance intensity image can characterize the chrominance effectively [49]. With the chrominance intensity image C, its MSCN coefficients can be computed as:

$$C'(x, y) = \frac{C(x, y) - \mu(x, y)}{\sigma(x, y) + 1} \tag{12}$$

with $C(x, y)$ and $C'(x, y)$ denoting the original and normalized values at position (x, y). $\mu(x, y)$ and $\sigma(x, y)$ stand for the mean and standard deviation of a local patch centered at (x, y), which are respectively calculated by:

$$\mu(x, y) = \sum_{s=-S}^{S} \sum_{t=-T}^{T} \omega_{s,t} C(x + s, y + t) \tag{13}$$

$$\sigma(x, y) = \sqrt{\sum_{s=-S}^{S} \sum_{t=-T}^{T} \omega_{s,t} [C(x+s, y+t) - x\mu(x, y)]^2} \tag{14}$$

where $\omega = \{\omega_{s,t} \mid s = -S, \ldots, S; t = -T, \ldots, T\}$ denotes a 2D circularly-symmetric Gaussian weighting filter. S and T are set to 3 in implementation. We further investigate the distribution of the obtained MSCN coefficients and find that it is modified by the contrast distortion, which can be exploited to describe the distortion level. To illustrate this fact, we show the distributions of MSCN coefficients of an original image and its contrast-distorted versions in Fig. 5. The original and the contrast-distorted images are the images shown in Fig. 2. It's clearly to see that the distributions of the contrast-distorted images are all discrepant from the original one, which indicates the capability of the MSCN coefficients distribution in characterizing the contrast distortion.

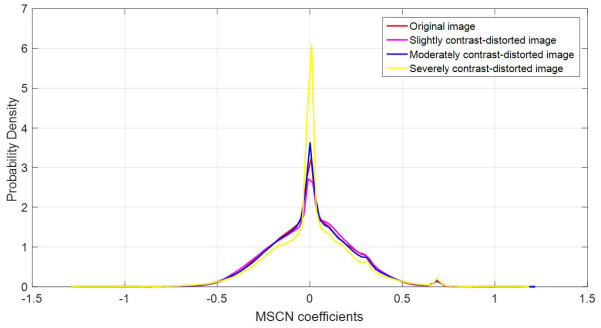

FIGURE 5. The chrominance MSCN distributions of the original, slightly contrast-distorted, moderately contrast-distorted, severely contrast-distorted images.

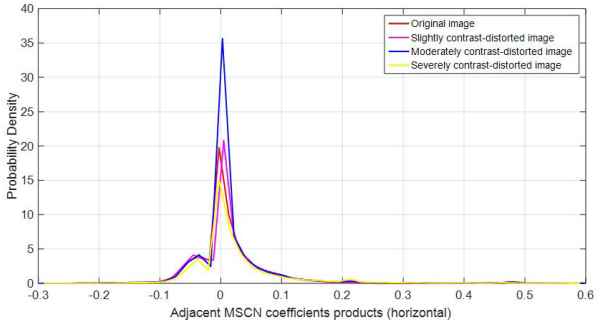

FIGURE 6. The distributions of the products of the chrominance adjacent MSCN coefficients along the horizontal direction of the original, slightly contrast-distorted, moderately contrast-distorted, severely contrast-distorted images.

To depict the MSCN coefficients distribution and thereby extract quality-aware features, we model the MSCN distribution with the zero-mean generalized Gaussian distribution (GGD), which is defined as:

$$g(x; \alpha, \beta) = \frac{\alpha}{2\beta\Gamma(1/\alpha)} \exp\left(-\left(\frac{|x|}{\beta}\right)^{\alpha}\right) \tag{15}$$

where $\Gamma(\cdot)$ refers to the gamma function, defined as:

$$\Gamma(x) = \int_0^{\infty} \phi^{x-1} e^{-\phi} d\phi, \quad x > 0 \tag{16}$$

where α and β are the GGD parameters. Accordingly, we extract α, β and the skewness and kurtosis features that depict the distribution precisely and employ them as our quality-aware features to characterize the image quality.

Furthermore, the products of pairs of the adjacent MSCN coefficients are also powerful to characterize the image quality [23]. Therefore, we further calculate the products of the adjacent chrominance MSCN coefficients along horizontal, vertical, main-diagonal and second-diagonal directions. In Fig. 6, we also show the distributions of the products of the adjacent chrominance MSCN coefficients along the horizontal direction of the original and the contrast-distorted images exhibited in Fig. 2. The deviations of the distributions of the contrast-distorted images from the original one can be clearly observed. In addition, as indicated in [23], each of

FIGURE 7. Some contrast-distorted image samples from the CCID2014 database.

TABLE 1. Summary of the quality-aware features.

Index	Category	Number
1	Spatial features	2
2	Histogram features	1
3	Perceptual features	1
4	Chrominance features	28

these four products can be modeled suitably with the zero mode asymmetric GGD (AGGD):

$$g(x;\gamma,\beta_l,\beta_r) = \begin{cases} \frac{\gamma}{(\beta_l+\beta_r)\Gamma(\frac{1}{\gamma})}\exp\left(-\left(\frac{-x}{\beta_l}\right)^{\gamma}\right) & \forall x \le 0 \\ \frac{\gamma}{(\beta_l+\beta_r)\Gamma(\frac{1}{\gamma})}\exp\left(-\left(\frac{x}{\beta_r}\right)^{\gamma}\right) & \forall x > 0 \end{cases} \tag{17}$$

The mean of this distribution is defined as:

$$\eta = (\beta_r - \beta_l)\frac{\Gamma(\frac{2}{\gamma})}{\Gamma(\frac{1}{\gamma})} \tag{18}$$

Likewise, the informative model parameters $(\gamma, \beta_l, \beta_r, \eta)$ of the AGGD and the skewness and kurtosis values are also estimated and introduced into our quality-aware features.

E. QUALITY EVALUATION

Up to now, we have addressed all the quality-aware features that characterize the contrast distortion in the image comprehensively. For convenient reading, we deliver a brief summary of the employed features in Table 1. It's easy to see that the total number of the quality-aware features is $(2+1+1+28) = 32$. To infer the quality of the contrast-distorted image, a mapping from the quality-aware features to the image quality score is needed to be learned. In this work, we employ SVR to learn the mapping function as it's highly effective in handling high dimensional data [50] and has been widely adopted in the NR IQA researches [23], [41], [51]. In implementation, we use the LIBSVM package with a radial basis function (RBF) kernel [52] to learn the NR model for quality evaluation.

III. EXPERIMENTAL RESULTS

A. EXPERIMENTAL PROTOCOL AND TESTING DATABASES

To quantify the prediction performance of the objective IQA methods, we employ four statistical indexes, which are Spearman Rank order Correlation coefficient (SRCC), Kendallạ́s rank correlation coefficient (KRCC), Pearsons linear correlation coefficient (PLCC) and root mean square error (RMSE). These four indexes are computed between the subjective scores and the objective scores given by the objective IQA algorithms. The SRCC, KRCC and PLCC values of a superior objective IQA method should be as close to 1 as possible, while the RMSE value should be as close to 0 as possible. It's also needed to point out that before calculating these above indexes, the objective scores are suggested to be fitted to the subjective scores through a five-parameter logistic function [53], defined as:

$$q(s) = \beta_1\left(\frac{1}{2} - \frac{1}{1+\exp(\beta_2\cdot(s-\beta_3))}\right) + \beta_4\cdot s + \beta_5 \tag{19}$$

where s refers to the objective score, $q(s)$ refers to the nonlinearly fitted score, $\beta_1 \sim \beta_5$ are the model parameters which are estimated through nonlinear fitting.

We conducted experiments on three standard contrast-distorted image databases/datasets. The first one is the CCID2014 database [35], which is a dedicated contrast-distorted image database and contains a total of 655 contrast-distorted images. The second one is the contrast-distorted dataset of the TID2013 image database [54], which contains 125 contrast-distorted images. The third one is the contrast-distorted dataset of the CSIQ database [55], which includes 116 contrast-distorted images. For illustration, we show some examples of the contrast-distorted images from the CCID2014 database in Fig. 7. It's apparent that contrast distortion can affect the image quality significantly.

B. IMPLEMENTATION SETTINGS

In sparse representation, for extracting the perceptual features, we set the dimension B_s of the image patch vector to be 64. The DCT dictionary of 64×144 that contains a total of 144 atoms was utilized as the over-complete dictionary $\mathbf{D}$ for sparse representation. We employed the Orthogonal Matching Pursuit (OMP) algorithm [56] to solve

TABLE 2. Prediction performance comparison on CCID2014, TID2013 and CSIQ databases. The best performance in each IQA algorithm category is highlighted with boldface.

Database	Index	FR methods			RR methods				NR methods				
		PSNR	SSIM	PCQI	RRED	FSI	RIQMC	QMC	NIQE	SNP-NIQE	BIQME	[32]	BCIQM (pro.)
CCID2014	SRCC	0.6879	0.8110	**0.8615**	0.6583	0.5983	0.8417	**0.8703**	0.3691	0.4269	0.8274	0.7873	**0.8851**
	KRCC	0.4940	0.6076	**0.6746**	0.4712	0.4269	0.6492	**0.6893**	0.2540	0.2923	0.6298	0.5766	**0.7062**
	PLCC	0.6071	0.8187	**0.8878**	0.7085	0.7274	0.8689	**0.8973**	0.4328	0.5113	0.8596	0.8008	**0.8969**
	RMSE	0.5148	0.3737	**0.2995**	0.4589	0.4467	0.3222	**0.2873**	0.5866	0.5596	0.3326	0.3899	**0.2876**
TID2013	SRCC	0.4458	0.3193	**0.8764**	0.3909	0.5182	**0.8477**	0.7553	0.1636	0.1957	0.7831	0.6850	**0.8816**
	KRCC	0.3107	0.2356	**0.7306**	0.3157	0.3834	**0.6616**	0.5717	0.1150	0.1348	0.5949	0.5084	**0.7285**
	PLCC	0.4423	0.5435	**0.9479**	0.6150	0.7706	**0.8433**	0.7418	0.2974	0.3181	0.8510	0.7256	**0.9265**
	RMSE	1.0259	0.9426	**0.3588**	0.8864	0.7572	**0.6210**	0.7783	1.1050	1.0942	0.5998	0.7877	**0.4190**
CSIQ	SRCC	0.8644	0.7799	**0.9407**	0.9269	0.9451	**0.9491**	0.9461	0.2359	0.3940	0.7681	0.7470	**0.8402**
	KRCC	0.6754	0.5895	**0.8181**	0.7906	0.8287	**0.8366**	0.8284	0.1702	0.2877	0.5969	0.5590	**0.6608**
	PLCC	0.8523	0.8010	**0.9550**	0.9453	**0.9643**	0.8905	0.9602	0.4809	0.5016	0.8144	0.7763	**0.8659**
	RMSE	0.0853	0.0933	**0.0489**	0.0528	**0.0426**	0.0697	0.0453	0.1513	0.1402	0.0911	0.1020	**0.0816**

the optimization problem defined in Eq.(7) and obtain the sparse vector. Detailed sparse representation configurations can be referred to in [14]. For estimating the model parameters in Eq.(15) and Eq.(17), we employed the moment matching-based method proposed in [57].

C. PREDICTION PERFORMANCE EVALUATION

We compare the proposed BCIQM with eleven state-of-the-art IQA methods, which are PSNR, SSIM [2], PCQI [36], RRED [4], FSI [14], RIQMC [35], QMC [58], NIQE [26], SNP-NIQE [7], BIQME [31] and [32]. Among them, PSNR, SSIM and PCQI belong to the FR IQA methods, RRED, FSI, RIQMC, QMC belong to the RR IQA methods, NIQE, SNP-NIQE, BIQME and [32] are the NR IQA methods. In addition, PCQI, RIQMC, QMC, BIQME, [32] and the proposed BCIQM are the dedicated quality methods for the contrast-distorted images, other models are the general-purpose IQA methods. As the proposed BCIQM and [32] need to train a quality model, we randomly partitioned each testing database into two parts. One is the training part which includes 80% images for training the quality module. The other one is the testing part that is composed of the remaining 20% images. Therefore, the training part and the testing part are non-overlapped. We trained the proposed BCIQM and [32] on the training part and tested them on the testing part. Such 80% train-20% test procedure was repeated 1000 times for avoiding bias. For the other compared methods that don't require training, we only test them on the testing part, which were also repeated 1000 times. The mean results over 1000-time tests of all the methods are listed in Table 2, where the best performance in the FR, RR and NR categories is highlighted with boldface, respectively.

From the results shown in Table 2, we can draw the following meaningful conclusions. Although PSNR and SSIM are the most widely adopted IQA metrics, they can only achieve moderate performance on the CCID2014 and CSIQ databases and even poor performance on the TID2013 database. By comparison, the dedicated PCQI metric for the contrast-distorted image can achieve much better prediction performance. Similarly, the general-purpose RRED and FSI methods perform unfavorably on the CCID2014 and TID2013 databases. While the specialized RIQMC and QMC methods perform much better across these three databases. For the NR methods, it's observed that the general-purpose NIQE and SNP-NIQE are also not good at evaluating the quality of the contrast-distorted image. In addition, although BIQME and [32] are the dedicated IQA methods for the contrast-distorted images, they still only achieve moderate performance. By comparison, the proposed BCIQM outperforms them by a large margin on each database. Furthermore, BCIQM can even achieve more promising performance than the FR PCQI approach on the largest CCID2014 database. These experiments clearly demonstrate the high effectiveness and superiority of the proposed BCIQM in evaluating the quality of the contrast-distorted images.

D. STATISTICAL SIGNIFICANCE TEST

For further examining the statistical significance of the objective IQA methods, we employed t-test on the prediction residuals between the nonlinearly-fitted objective scores and the subjective scores. The experimental results are listed in Table 3, where the symbols of "1", "0" and "−1" respectively denote that the proposed BCIQM is statistically superior, comparative and inferior to the compared objective methods with 95% confidence. From this table, we observe that the proposed BCIQM is only comparative with the RR method QMC on the CCID2014 database. It is superior to all the other competitors on the CCID2014 database. On the TID2013 database, BCIQM is only inferior to the FR PCQI method. While on the CSIQ database, BCIQM is inferior to PCQI, RRED, FSI, RIQMC and QMC methods. For the NR methods, BCIQM is consistently superior to all the other NR methods on each database, which demonstrates the advantage of BCIQM in quantifying the image quality statistically.

TABLE 3. T-test results on CCID2014, TID2013 and CSIQ Databases.

Database	FR methods			RR methods				NR methods			
	PSNR	SSIM	PCQI	RRED	FSI	RIQMC	QMC	NIQE	SNP-NIQE	BIQME	[32]
CCID2014	1	1	1	1	1	1	0	1	1	1	1
TID2013	1	1	-1	1	1	1	1	1	1	1	1
CSIQ	1	1	-1	-1	-1	-1	-1	1	1	1	1

TABLE 4. Experimental results of ablation study measured by SRCC on CCID2014, TID2013 and CSIQ databases.

Feature type / Database	S	H	P	C	S, H	S, P	S, C	H, P
CCID2014	0.5305	0.6061	0.5676	0.7436	0.7220	0.6027	0.8227	0.7885
TID2013	0.4751	0.6979	0.4625	0.6881	0.8048	0.5014	0.7162	0.7819
CSIQ	0.5961	0.7419	0.5980	0.6166	0.8175	0.6314	0.6367	0.8049
Feature type / Database	**H, C**	**P, C**	**S, H, P**	**S, H, C**	**S, P, C**	**H, P, C**	**S, H, P, C**	
CCID2014	0.8392	0.7660	0.8268	0.8651	0.8566	0.8742	0.8851	
TID2013	0.8175	0.7013	0.8287	0.8593	0.8648	0.8689	0.8816	
CSIQ	0.8225	0.6561	0.8293	0.8306	0.8281	0.8313	0.8402	

TABLE 5. Average running time of the IQA methods.

Methods	PSNR	SSIM	PCQI	RRED	FSI	RIQMC	QMC	NIQE	SNP-NIQE	BIQME	[32]	BCIQM (pro.)
Time (s)	0.005	0.201	0.193	1.906	4.136	8.504	0.051	0.848	3.626	3.192	0.391	2.284

E. ABLATION STUDY

It's interesting to understand the contribution of different types of features of BCIQM in characterizing the image quality. Therefore, we performed ablation study on the three databases. Specifically, we used each type of the quality-aware features and their combinations to construct the quality prediction model respectively and then tested their prediction performance. The experimental methodologies were set the same as that in Section III-C. The prediction performance measured by SRCC of each type of the features and their combinations is reported in Table 4, where we use "S", "H", "P", "C" to represent the extracted Spatial, Histogram, Perceptual and Chrominance features, respectively.

From this table, we can have the following enlightening conclusions. First, the spatial features and the perceptual features play comparative roles in characterizing the image quality, which can only lead to moderate prediction performance by themselves. Second, the histogram features can achieve higher performance, which confirms that the proper characterization of the image histogram can provide a good measure for the quality of the contrast-distorted images. Third, it's interesting to find that the performance of the chrominance features is also promising, which demonstrates that the chrominance of the image does affect the image quality and characterization of the chrominance is very necessary for image quality evaluation. Fourth, we observe that if one feature is more effective than the other one feature, then the feature combined with other features can be more effective than the other one feature combined with the same features in most cases. For example, as shown in Table 4, the chrominance feature (C) is more effective than the perceptual feature (P). Accordingly, the performance of the combination "S, C" is higher than that of the combination "S, P", the performance of the combination "H, C" is higher than that of "H, P" and the performance of the combination "S, H, C" is also higher than that of "S, H, P". These results reveal that the combination of features maintains the contribution of the combined features well. Fifth, the combination of the features can outperform each type of the combined features. For example, the performance of the combination "S, H" is higher than that of "S" and "H". The performance of the combination "S, H, P" is observed to be higher than that of "S", "H", "P", "S, H", "S, P" and "H, P". The combination of "S, H, P, C" that contains all types of the quality-aware features achieves the best prediction performance. These observations fully demonstrate that the designed features in BCIQM play complementary roles in characterizing the image quality.

F. TIME COMPLEXITY

At last, we examined the time complexity of the proposed BCIQM, which is an important index for practical applications. For comparison, we also include the other IQA algorithms. Specifically, we ran all the IQA methods on the entire CCID2014 database and the average running time of each method was recorded. Notice that our hardware platform is Thinkpad X220 computer with 2.5GHz CPU and 4G RAM.

The software platform is Matlab R2015b. The resolution of the images in CCID2014 database is 768 × 512. We list the average running time measured by seconds in Table 5. It's clearly to see that the average running time of PSNR, SSIM, PCQI, QMC, NIQE and [32] is less than one second, which is very promising. While the running time of the proposed BCIQM is 2.284 seconds, which is also acceptable for image applications.

IV. CONCLUSION

In this paper, we investigated the issue of blindly evaluating the quality of the contrast-distorted images and have proposed a novel dedicated NR IQA approach, named BCIQM. In BCIQM, we designed a set of quality-aware features from the image spatial domain, image histogram, visual perception and chrominance respectively, which can characterize the image quality comprehensively and thus more precisely. Then we employed SVR to integrate all the extracted features and infer the image quality score. Extensive experiments conducted on three standard contrast-distorted image databases/datasets, i.e., CCID2014, TID2013 and CSIQ, demonstrate that the proposed BCIQM achieves very promising performance on evaluating the quality of the contrast-distorted images.

REFERENCES

[1] Y. Liu, G. Zhai, D. Zhao, and X. Liu, "Frame rate and perceptual quality for HD video," in *Proc. Pacific Rim Conf. Multimedia (PCM)*, 2015, pp. 497–505.
[2] Z. Wang, A. C. Bovik, H. R. Sheikh, and E. P. Simoncelli, "Image quality assessment: From error visibility to structural similarity," *IEEE Trans. Image Process.*, vol. 13, no. 4, pp. 600–612, Apr. 2004.
[3] Y. Liu, G. Zhai, X. Liu, and D. Zhao, "Perceptual image quality assessment combining free-energy principle and sparse representation," in *Proc. IEEE Int. Symp. Circuits Syst. (ISCAS)*, May 2016, pp. 1586–1589.
[4] R. Soundararajan and A. C. Bovik, "RRED indices: Reduced reference entropic differencing for image quality assessment," *IEEE Trans. Image Process.*, vol. 21, no. 2, pp. 517–526, Feb. 2012.
[5] G. Zhai, X. Wu, X. Yang, W. Lin, and W. Zhang, "A psychovisual quality metric in free-energy principle," *IEEE Trans. Image Process.*, vol. 21, no. 1, pp. 41–52, Jan. 2012.
[6] J. Wu, Y. Liu, L. Li, and G. Shi, "Attended visual content degradation based reduced reference image quality assessment," *IEEE Access*, vol. 6, pp. 12493–12504, 2018.
[7] Y. Liu, K. Gu, Y. Zhang, X. Li, G. Zhai, D. Zhao, and W. Gao, "Unsupervised blind image quality evaluation via statistical measurements of structure, naturalness, and perception," *IEEE Trans. Circuits Syst. Video Technol.*, vol. 30, no. 4, pp. 929–943, Apr. 2020.
[8] X. Min, K. Gu, G. Zhai, J. Liu, X. Yang, and C. W. Chen, "Blind quality assessment based on pseudo-reference image," *IEEE Trans. Multimedia*, vol. 20, no. 8, pp. 2049–2062, Aug. 2018.
[9] X. Min, K. Ma, K. Gu, G. Zhai, Z. Wang, and W. Lin, "Unified blind quality assessment of compressed natural, graphic, and screen content images," *IEEE Trans. Image Process.*, vol. 26, no. 11, pp. 5462–5474, Nov. 2017.
[10] L. Zhang, L. Zhang, X. Mou, and D. Zhang, "FSIM: A feature similarity index for image quality assessment," *IEEE Trans. Image Process.*, vol. 20, no. 8, pp. 2378–2386, Aug. 2011.
[11] L. Zhang, Y. Shen, and H. Li, "VSI: A visual saliency-induced index for perceptual image quality assessment," *IEEE Trans. Image Process.*, vol. 23, no. 10, pp. 4270–4281, Oct. 2014.
[12] K. Gu, L. Li, H. Lu, X. Min, and W. Lin, "A fast reliable image quality predictor by fusing micro-and macro-structures," *IEEE Trans. Ind. Electron.*, vol. 64, no. 5, pp. 3903–3912, May 2017.
[13] Z. Wang, G. Wu, H. R. Sheikh, E. P. Simoncelli, E.-H. Yang, and A. C. Bovik, "Quality-aware images," *IEEE Trans. Image Process.*, vol. 15, no. 6, pp. 1680–1689, Jun. 2006.
[14] Y. Liu, G. Zhai, K. Gu, X. Liu, D. Zhao, and W. Gao, "Reduced-reference image quality assessment in free-energy principle and sparse representation," *IEEE Trans. Multimedia*, vol. 20, no. 2, pp. 379–391, Feb. 2018.
[15] X. Min, K. Gu, G. Zhai, M. Hu, and X. Yang, "Saliency-induced reduced-reference quality index for natural scene and screen content images," *Signal Process.*, vol. 145, pp. 127–136, Apr. 2018.
[16] W. Zhu, G. Zhai, X. Min, M. Hu, J. Liu, G. Guo, and X. Yang, "Multi-channel decomposition in tandem with free-energy principle for reduced-reference image quality assessment," *IEEE Trans. Multimedia*, vol. 21, no. 9, pp. 2334–2346, Sep. 2019.
[17] Y. Fang, J. Yan, J. Wang, X. Liu, G. Zhai, and P. Le Callet, "Learning a no-reference quality predictor of stereoscopic images by visual binocular properties," *IEEE Access*, vol. 7, pp. 132649–132661, 2019.
[18] Y. Liu, K. Gu, S. Wang, D. Zhao, and W. Gao, "Blind quality assessment of camera images based on low-level and high-level statistical features," *IEEE Trans. Multimedia*, vol. 21, no. 1, pp. 135–146, Jan. 2019.
[19] L. Li, Y. Yan, Z. Lu, J. Wu, K. Gu, and S. Wang, "No-reference quality assessment of deblurred images based on natural scene statistics," *IEEE Access*, vol. 5, pp. 2163–2171, 2017.
[20] X. Min, G. Zhai, K. Gu, Y. Zhu, J. Zhou, G. Guo, X. Yang, X. Guan, and W. Zhang, "Quality evaluation of image dehazing methods using synthetic hazy images," *IEEE Trans. Multimedia*, vol. 21, no. 9, pp. 2319–2333, Sep. 2019.
[21] M. A. Saad, A. C. Bovik, and C. Charrier, "Blind image quality assessment: A natural scene statistics approach in the DCT domain," *IEEE Trans. Image Process.*, vol. 21, no. 8, pp. 3339–3352, Aug. 2012.
[22] A. K. Moorthy and A. C. Bovik, "Blind image quality assessment: From natural scene statistics to perceptual quality," *IEEE Trans. Image Process.*, vol. 20, no. 12, pp. 3350–3364, Dec. 2011.
[23] A. Mittal, A. K. Moorthy, and A. C. Bovik, "No-reference image quality assessment in the spatial domain," *IEEE Trans. Image Process.*, vol. 21, no. 12, pp. 4695–4708, Dec. 2012.
[24] C. Li, Y. Zhang, X. Wu, and Y. Zheng, "A multi-scale learning local phase and amplitude blind image quality assessment for multiply distorted images," *IEEE Access*, vol. 6, pp. 64577–64586, 2018.
[25] X. Min, G. Zhai, K. Gu, Y. Liu, and X. Yang, "Blind image quality estimation via distortion aggravation," *IEEE Trans. Broadcast.*, vol. 64, no. 2, pp. 508–517, Jun. 2018.
[26] A. Mittal, R. Soundararajan, and A. C. Bovik, "Making a 'completely blind' image quality analyzer," *IEEE Signal Process. Lett.*, vol. 20, no. 3, pp. 209–212, Mar. 2013.
[27] W. Xue, L. Zhang, and X. Mou, "Learning without human scores for blind image quality assessment," in *Proc. IEEE Conf. Comput. Vis. Pattern Recognit.*, Jun. 2013, pp. 995–1002.
[28] K. Ma, W. Liu, T. Liu, Z. Wang, and D. Tao, "DipIQ: Blind image quality assessment by learning-to-rank discriminable image pairs," *IEEE Trans. Image Process.*, vol. 26, no. 8, pp. 3951–3964, Aug. 2017.
[29] Q. Yan, D. Gong, and Y. Zhang, "Two-stream convolutional networks for blind image quality assessment," *IEEE Trans. Image Process.*, vol. 28, no. 5, pp. 2200–2211, May 2019.
[30] J. Kim, A.-D. Nguyen, and S. Lee, "Deep CNN-based blind image quality predictor," *IEEE Trans. Neural Netw. Learn. Syst.*, vol. 30, no. 1, pp. 11–24, Jan. 2019.
[31] K. Gu, D. Tao, J.-F. Qiao, and W. Lin, "Learning a no-reference quality assessment model of enhanced images with big data," *IEEE Trans. Neural Netw. Learn. Syst.*, vol. 29, no. 4, pp. 1301–1313, Apr. 2018.
[32] Y. Fang, K. Ma, Z. Wang, W. Lin, Z. Fang, and G. Zhai, "No-reference quality assessment of contrast-distorted images based on natural scene statistics," *IEEE Signal Process. Lett.*, vol. 22, no. 7, pp. 838–842, Jul. 2015.
[33] Y. Zhu, G. Zhai, and X. Min, "The prediction of head and eye movement for 360 degree images," *Signal Process., Image Commun.*, vol. 69, pp. 15–25, Nov. 2018.
[34] Y. Zhu, G. Zhai, X. Min, and J. Zhou, "The prediction of saliency map for head and eye movements in 360 degree images," *IEEE Trans. Multimedia*, early access, Dec. 12, 2019, doi: 10.1109/TMM.2019.2957986.
[35] K. Gu, G. Zhai, W. Lin, and M. Liu, "The analysis of image contrast: From quality assessment to automatic enhancement," *IEEE Trans. Cybern.*, vol. 46, no. 1, pp. 284–297, Jan. 2016.

[36] S. Wang, K. Ma, H. Yeganeh, Z. Wang, and W. Lin, "A patch-structure representation method for quality assessment of contrast changed images," *IEEE Signal Process. Lett.*, vol. 22, no. 12, pp. 2387–2390, Dec. 2015.
[37] K. Gu, W. Lin, G. Zhai, X. Yang, W. Zhang, and C. W. Chen, "No-reference quality metric of contrast-distorted images based on information maximization," *IEEE Trans. Cybern.*, vol. 47, no. 12, pp. 4559–4565, Dec. 2017.
[38] K. Friston, J. Kilner, and L. Harrison, "A free energy principle for the brain," *J. Physiol. Paris*, vol. 100, no. 1, pp. 70–87, 2006.
[39] Y. Zhao, Y. Liu, F. Jiang, X. Liu, and D. Zhao, "Fast noisy image quality assessment based on free-energy principle," in *Proc. Int. Forum Digit. TV Wireless Multimedia Commun.*, 2018, pp. 290–299.
[40] K. Friston, "The free-energy principle: A unified brain theory?" *Nature Rev. Neurosci.*, vol. 11, no. 2, pp. 127–138, Feb. 2010.
[41] K. Gu, G. Zhai, X. Yang, and W. Zhang, "Using free energy principle for blind image quality assessment," *IEEE Trans. Multimedia*, vol. 17, no. 1, pp. 50–63, Jan. 2015.
[42] B. A. Olshausen and D. J. Field, "Sparse coding with an overcomplete basis set: A strategy employed by V1?" *Vis. Res.*, vol. 37, no. 23, pp. 3311–3325, Dec. 1997.
[43] B. A. Olshausen and D. J. Field, "Emergence of simple-cell receptive field properties by learning a sparse code for natural images," *Nature*, vol. 381, no. 6583, pp. 607–609, Jun. 1996.
[44] B. A. Olshausen and D. J. Field, "How close are we to understanding V1?" *Neural Comput.*, vol. 17, no. 8, pp. 1665–1699, Aug. 2005.
[45] B. Olshausen and D. Field, "Vision and the coding of natural images," *Amer. Sci.*, vol. 88, no. 3, p. 238, 2000.
[46] B. A. Olshausen, "Principles of image representation in visual cortex," *Vis. Neurosci.*, vol. 2, pp. 1603–1615, Feb. 2003.
[47] Y. Liu, K. Gu, G. Zhai, X. Liu, D. Zhao, and W. Gao, "Quality assessment for real out-of-focus blurred images," *J. Vis. Commun. Image Represent.*, vol. 46, pp. 70–80, Jul. 2017.
[48] U. Rajashekar, Z. Wang, and E. P. Simoncelli, "Perceptual quality assessment of color images using adaptive signal representation," *Proc. SPIE, Hum. Vis. Electron. Imag.*, vol. 7527, Feb. 2010, Art. no. 75271L.
[49] D. Ghadiyaram and A. C. Bovik, "Perceptual quality prediction on authentically distorted images using a bag of features approach," *J. Vis.*, vol. 17, no. 1, p. 32, Jan. 2017.
[50] C. J. C. Burges, "A tutorial on support vector machines for pattern recognition," *Data Mining Knowl. Discovery*, vol. 2, no. 2, pp. 121–167, 1998.
[51] Q. Li, W. Lin, J. Xu, and Y. Fang, "Blind image quality assessment using statistical structural and luminance features," *IEEE Trans. Multimedia*, vol. 18, no. 12, pp. 2457–2469, Dec. 2016.
[52] C.-C. Chang and C.-J. Lin, "LIBSVM: A library for support vector machines," *ACM Trans. Intell. Syst. Technol.*, vol. 2, no. 3, pp. 27:1–27:27, Apr. 2011. [Online]. Available: http://www.csie.ntu.edu.tw/~cjlin/libsvm
[53] A. M. Rohaly, J. Libert, P. Corriveau, and A. Webster, *Final Report From the Video Quality Experts Group on the Validation of Objective Models of Video Quality Assessment*, Standard, ITU-T Standards Contribution COM, 2000, pp. 9–80. [Online]. Available: https://pan.baidu.com/s/1akAWiuQlM6SKnYT912mQSA
[54] N. Ponomarenko, O. Ieremeiev, V. Lukin, K. Egiazarian, L. Jin, J. Astola, B. Vozel, K. Chehdi, M. Carli, and F. Battisti, "Color image database TID2013: Peculiarities and preliminary results," in *Proc. 4th Eur. Workshop Vis. Inf. Process.*, 2013, pp. 106–111.
[55] E. C. Larson and D. Chandler. (2010). *Categorical Image Quality (CSIQ) Database*. [Online]. Available: http://vision.okstate.edu/csiq
[56] J. A. Tropp and A. C. Gilbert, "Signal recovery from random measurements via orthogonal matching pursuit," *IEEE Trans. Inf. Theory*, vol. 53, no. 12, pp. 4655–4666, Dec. 2007.
[57] K. Sharifi and A. Leon-Garcia, "Estimation of shape parameter for generalized Gaussian distributions in subband decompositions of video," *IEEE Trans. Circuits Syst. Video Technol.*, vol. 5, no. 1, pp. 52–56, Feb. 1995.
[58] K. Gu, G. Zhai, X. Yang, W. Zhang, and C. Wen Chen, "Automatic contrast enhancement technology with saliency preservation," *IEEE Trans. Circuits Syst. Video Technol.*, vol. 25, no. 9, pp. 1480–1494, Sep. 2015.

YUTAO LIU received the B.S., M.S., and Ph.D. degrees in computer science from the Harbin Institute of Technology (HIT), Harbin, China, in 2011, 2013, and 2018, respectively. From 2014 to 2016, he was with the Institute of Image Communication and Information Processing, Shanghai Jiao Tong University, Shanghai, as a Research Assistant. He is currently a Postdoctoral Fellow with Tsinghua Shenzhen International Graduate School. His research interests include image quality assessment, perceptual image processing, and computer vision.

XIU LI (Member, IEEE) received the Ph.D. degree in computer integrated manufacturing in 2000. Since then, she has been worked with Tsinghua University. Her research interests are in the areas of data mining, deep learning, computer vision, and image processing.